International Journal of Applied Power Engineering (IJAPE)
Vol.7, No.1, April 2018, pp. 73~86
ISSN: 2252-8792 DOI: 10.11591/ijape.v7.i1.pp73-86

Localized Transient Stability (LTS) Method for Real-time Localized Control

Abdul Malek Miah
Department of Industrial & Electrical Engineering Technology, South Carolina State University, USA

Article Info

Article history:

Received Oct 5, 2017
Revised Mar 8, 2018
Accepted Mar 30, 2018

Keyword:

Localized power system
Localized transient stability
Power system dynamics
Real-time localized control
Transient stability control

ABSTRACT

Very recently, a new methodology was introduced solely for the purpose of real-time localized control of transient stability. The proposed new method is based on the localized transient stability of a power system. This is completely a new idea in transient stability. In this method, the post-fault power system is represented by a two-generator localized power system at the site of each individual generator. If each of these localized power systems reaches its respective stable equilibrium, then the full power system also reaches its stable equilibrium. Therefore, in terms of real-time localized control of transient stability, if each of the localized power systems is driven to its respective stable equilibrium by local control actions with local computations using the locally measured data, then the full power system is driven to its stable equilibrium. Thus the method can be easily implemented for real-time localized control of transient stability. In this paper, the details of the mathematical formulations are presented. Some interesting test results on the well-known New England 39-bus 10-generator system are also presented in this paper to demonstrate the potential of the proposed method for use in real-time localized control of transient stability.

Corresponding Author:

Abdul Malek Miah,
Department of Industrial & Electrical Engineering Technology,
South Carolina State University,
300 College Street NE, Orangeburg, SC 29117, USA.
Email: amiah@scsu.edu

1. INTRODUCTION

Transient stability assessment and control are crucial for the secured operation of power systems. In the context of on-line applications, a number of computationally fast transient stability assessment methods have been reported in the literature. Among these, the direct methods such as the transient energy function method [1] and extended equal area criterion (EEAC) [2] are the important ones which have been implemented at some utility companies [3]. However, all the fast methods use classical representation of power systems and hence they are limited to short term assessment like the first swing stability. All these fast methods are faster than the standard step-by-step (SBS) numerical integration method which is considered as the most accurate method of transient stability assessment since this method can accommodate any degree of modeling of the power systems. The fast methods can be made even faster by coupling with them the dynamic equivalent reduction techniques [4-6]. Some recent developments in transient stability assessment are reported in [7-13]. There are also research efforts in using parallel processing [14-16] to speed up the transient stability simulations.

Besides the natural causes (hurricane, tornado, ice storm, earthquake, etc.), transient instability has been known to be a major cause for widespread power blackouts. Power blackout does not occur frequently, but when it does, the impacts can be devastating in terms of human sufferings and financial losses. Since a vast majority of U. S. agricultural farms rely on the electricity from power grids for their proper operation,

power blackouts can have disastrous effects in terms of significant losses of crops and livestock. Power blackouts can also cause substantial spoilage of refrigerated agricultural products. In addition, power blackouts can have serious impacts in terms of huge financial losses by the other businesses. Therefore, with the stressed transmission systems of today, real-time control of transient stability is critically important to avoid widespread power blackouts due to transient instability. However, all the transient stability methods require system-wide transfer of measurement data to the system control center for use in real-time control of transient stability. Due to the development of phasor measurement unit (PMU), there are research efforts for real-time transient stability assessment [17-21] using PMU measurements. There are also research efforts for real-time centralized control of transient stability [21-23] using control actions like tripping of generators, tripping of transmission lines, etc.

However, since real-time localized control of transient stability can be much simpler, faster and cheaper compared to the real-time centralized control, there are research efforts for localized controls. These localized controls use local computations with local information and measurements. To avoid the system-wide transfer of real-time measurement data, Local Equilibrium Frame (LEF) was suggested in [24] for the purpose of localized control. However, the equilibrium state in LEF refers to a state at which all the generators run at synchronous speed. This synchronous speed equilibrium condition is sufficient, but not necessary, as it is too restrictive. This is a serious drawback of LEF. The center-of-angle (COA) frame of reference in which the generator angles are with respect to the center of angles of all the generators, and the machine frame of reference in which the generator angles are with respect to the angle of a chosen common generator do not suffer from such drawback. The equilibrium state in these reference frames refers to a state at which all the generators run at the same speed that is not necessarily the synchronous speed. Further, LEF cannot provide any dynamic equation for the external system. This is another drawback of LEF. There are also a number of strategies [25-30] that have been suggested in the literature for localized control of transient stability using different control means like braking resistors, series capacitors, fast valving and FACTS devices. However, these strategies are developed using very simplified models for the external systems like the infinite bus. Therefore, in each of these strategies, equilibrium refers to synchronous speed equilibrium which is a serious drawback. A control strategy based on simplified model may work only for some special faults in a multi-machine power system [29]. In all these strategies, simplified models are used due to the lack of availability of a suitable dynamic model for the remaining generators and a methodology that can be implemented for localized control of transient stability in multi-machine power systems.

To overcome the drawbacks of localized control, a new methodology referred to as the Localized Transient Stability (LTS) Method is proposed here solely for the purpose of real-time localized control of transient stability. The proposed method is based on localized transient stability of a power system. This is completely a new idea. The method can be easily implemented for real-time localized control of transient stability. The system equilibrium state in the proposed method refers to a state at which all the generators run at the same speed that is not necessarily the synchronous speed. The method also provides dynamic equations for the remaining generators, which are necessary to design effective localized control strategies that can drive the power system to its appropriate equilibrium. Very recently, the proposed method was briefly introduced in [31]. However, in the present paper, the details of the mathematical formulations of the proposed method are presented. Some interesting test results on the very well-known New England 39-bus 10-generator system are also presented to demonstrate the potential of the proposed method for use in real-time localized control of transient stability.

2. METHEMATICAL FORMULATIONS OF THE PROPOSED METHOD

In the proposed method, transient stability is viewed as the interaction of each individual generator with its respective remaining generators. Therefore, the method uses two-generator localized models of the power system as it is seen from the sites of different individual generators. However, the development of a localized power system model involves the derivation of a simple dynamic equivalent for the remaining generators. This dynamic equivalent is obtained by satisfying the necessary nodal equation and generator swing equations. However, in the presence of a fault like the short circuit fault on the system, this dynamic equivalent is not available. Therefore, the proposed method uses the post-fault system. Note that the transient stability assessment and control are actually the assessment and control of the post-fault system. To develop the proposed method, a power system of n generators with classical representation is considered. However, since the classical model is used, the proposed method is limited to short term real-time control.

2.1. A simple dynamic equivalent for the remaining generators

To develop a simple dynamic equivalent for the remaining generators, at the site of an individual generator referred to as local generator, say the nth local generator, the post-fault power system network is

partitioned into two subsystems at the internal bus of the local generator: subsystem *C* containing the local generator, and subsystem *D* containing the remaining system. These two subsystems are connected to each other only at the internal bus of the local generator. Here, the interest is to form a dynamic equivalent for the subsystem *D* containing the remaining generators which may or may not be coherent. Therefore, this equivalent is a new kind of dynamic equivalent and is different from the coherency-based equivalents. The following sets of indices are defined.

$$C_I = \{n\}; \quad D_I = \{1, 2, \cdots, (n-1)\}$$

where C_I is the index for the local generator internal bus, and D_I are the indices for all the (n-1) remaining generator internal buses. After the power system network is reduced to the generator internal buses, the power system external to the local generator internal bus appears as in Figure 1. Here, $\mathbf{I}_n$=phasor current injected into area *D* at the local generator internal bus, $\mathbf{y}_k$ is a shunt admittance at an internal bus *k* that appears due to network reduction, $\mathbf{Y}_{ik}=\mathbf{Y}_{ki}=G_{ik}+jB_{ik}=G_{ki}+jB_{ki}$=elements of the reduced admittance matrix, and $\mathbf{E}_i=E_i\angle\delta_i$=phasor voltage of a generator internal bus. Further, M_i, δ_i and P_{mi} are respectively the inertia constant, rotor angle and mechanical input power of a generator. However, from the electrical network point of view, only the network shown in Figure 2(a) is seen by the local generator internal bus.

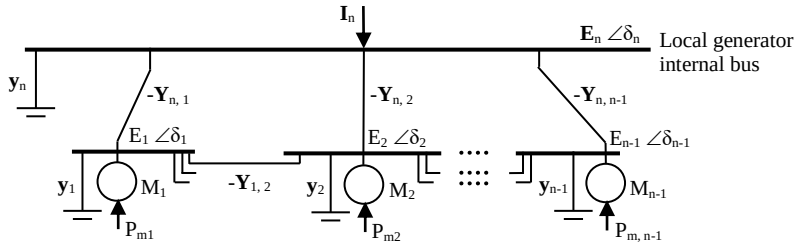

Figure 1. Remaining system *D* (the power system external to the local generator internal bus)

For the purpose of transient stability, area *D* in Figure 2(a) can now be described by one nodal equation at the local generator internal bus and (n-1) swing equations for the remaining generators. The nodal equation is written as

$$\mathbf{I}_n = \mathbf{Y}_{nn}\mathbf{E}_n + \sum_{k \in D_I} \mathbf{Y}_{nk}\mathbf{E}_k \tag{1}$$

which can also be rewritten as

$$\mathbf{I}_n = \mathbf{y}_n\mathbf{E}_n + \sum_{k \in D_I} \mathbf{Y}_{nk}(\mathbf{E}_k - \mathbf{E}_n) \tag{2a}$$

where

$$\mathbf{y}_n = \mathbf{Y}_{nn} + \sum_{k \in D_I} \mathbf{Y}_{nk} \tag{2b}$$

To satisfy the dynamic behavior of a remaining generator *i* in Figure 2(a), it is considered that this generator has its original inertia constant M_i. However, its electrical output power as seen in Figure 1 is decomposed into two components: first component is the power flowing towards the local generator; second component is the combination of the power flowing into the shunt admittance at the internal bus of this generator and the power flowing towards the other remaining generators. Now an equivalent mechanical input power P_i of this generator is defined as its original mechanical input power P_{mi} minus the second component of the decomposed power. This P_i as shown in Figure 2(a) produces the original post-fault trajectory of this generator. However, this mathematical manipulation makes P_i a time varying quantity unless all the remaining generators are coherent. The swing equations of the remaining generators in Figure 2(a) are now written in synchronous frame of reference as:

$$M_i \frac{d^2\delta_i}{dt^2} = P_i + E_i^2 G_{in} - E_i E_n [G_{in}\cos(\delta_i - \delta_n) + B_{in}\sin(\delta_i - \delta_n)] \quad \forall i \in D_I \tag{3}$$

To aggregate the generators of Figure 2(a) to one equivalent generator, the network enclosed by the dashed lines is replaced by its Thevenin equivalent. Figure 2(b) now becomes the single-generator dynamic equivalent of Figure 2(a).

In Figure 2(b), E_T, δ_T, M_T, and P_T are respectively the internal bus voltage magnitude, rotor angle, inertia constant, and mechanical input power of the equivalent generator. The nodal equation (2) now becomes

$$\mathbf{I}_n = \mathbf{y}_n \mathbf{E}_n - \mathbf{y}_T (\mathbf{E}_T - \mathbf{E}_n) \tag{4a}$$

where

$$\mathbf{y}_T = (g_T + jb_T) = -\sum_{k \in D_I} \mathbf{Y}_{nk} = -\sum_{k \in D_I} \mathbf{Y}_{kn} \tag{4b}$$

is the Thevenin admittance that appears between the local generator internal bus and the equivalent generator internal bus. To determine the internal voltage E_T and the rotor angle δ_T from the local generator internal bus quantities, (4a) can be written as

$$\mathbf{E}_T = (-\mathbf{I}_n + \mathbf{y}_n \mathbf{E}_n + \mathbf{y}_T \mathbf{E}_n) / \mathbf{y}_T \tag{5}$$

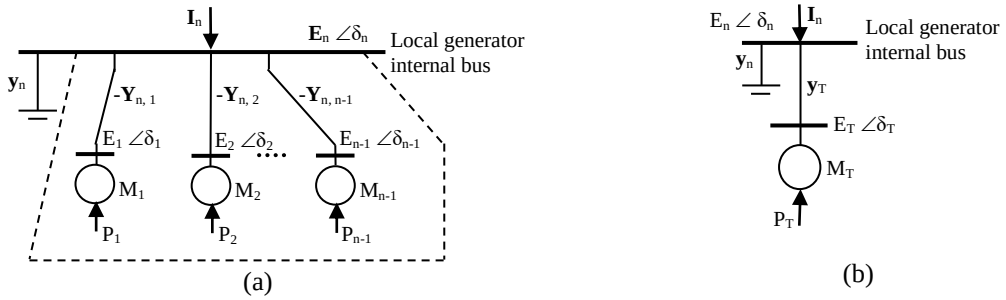

Figure 2. (a) Equivalent of remaining system *D* as seen by the local generator, (b) Single-generator dynamic equivalent of remaining system *D*

However, by comparing (2a) and (4a), $\mathbf{E}_T$ is given by

$$\mathbf{E}_T = E_T \angle \delta_T = (\sum_{k \in D_I} \mathbf{Y}_{nk} \mathbf{E}_k) / (\sum_{k \in D_I} \mathbf{Y}_{nk}) \tag{6}$$

which is the expression for the Thevenin phasor voltage. Equation (6) clearly indicates that $\mathbf{E}_T$ is an admittance-weighted aggregated average phasor voltage of all the remaining generator internal bus phasor voltages with the weighting admittances being the ones which connect the local generator internal bus with the remaining generator internal buses. Thus the angle of this aggregated average phasor voltage is taken as the rotor angle δ_T. Using (6), it can be shown that E_T is a time varying quantity unless all the remaining generators are coherent. The equivalent shown in Figure 2(b) can also be interpreted as the result of assigning the same aggregated average phasor voltage $\mathbf{E}_T = E_T \angle \delta_T$ to all the remaining generator internal buses in Figure 2(a) and then forming the Thevenin equivalent. It can be easily shown that the Thevenin equivalent remains unaltered when all the remaining generator internal buses are assigned the same aggregated average phasor voltage $\mathbf{E}_T = E_T \angle \delta_T$. Therefore, the swing equation for the equivalent generator is obtained by replacing all the remaining generator internal bus voltages i.e. $\mathbf{E}_i = E_i \angle \delta_i \ \forall i \in D_I$ by $\mathbf{E}_T = E_T \angle \delta_T$ in the swing equations (3) and then summing them. The resulting swing equation for the equivalent generator is thus given by

$$(\sum_{i\in D_l} M_i)\frac{d^2\delta_T}{dt^2} = \sum_{i\in D_l} P_i + E_T^2 \sum_{i\in D_l} G_{in} - E_T E_n[(\sum_{i\in D_l} G_{in})\cos(\delta_T - \delta_n) + (\sum_{i\in D_l} B_{in})\sin(\delta_T - \delta_n)] \quad (7)$$

which can be written as

$$\frac{d^2\delta_T}{dt^2} M_T = P_T - E_T^2 g_T + E_T E_n[g_T \cos(\delta_T - \delta_n) + b_T \sin(\delta_T - \delta_n)] \quad (8a)$$

with the inertia constant M_T and mechanical input power P_T of the equivalent generator given by

$$M_T = \sum_{i\in D_l} M_i, \qquad P_T = \sum_{i\in D_l} P_i \quad (8b)$$

In this aggregation, since the internal phasor voltages of the remaining generators are replaced by a common aggregated average phasor voltage, the real power at the internal bus of the equivalent generator is expected to be approximately equal to the sum of the real powers at the internal buses of all the remaining generators, i.e.

$$\begin{aligned} &E_T^2 g_T - E_T E_n[g_T \cos(\delta_T - \delta_n) + b_T \sin(\delta_T - \delta_n)] \\ &\quad = -\sum_{i\in D_l} E_i^2 G_{in} + \sum_{i\in D_l} E_i E_n[G_{in}\cos(\delta_i - \delta_n) + B_{in}\sin(\delta_i - \delta_n)] \end{aligned} \quad (9)$$

The equivalent presented here is a localized model that represents the dynamic behavior of the remaining generators as seen at the site of the local generator, but P_T and E_T in this model are in general time varying quantities.

2.2. Post-fault localized power system model

The power system as seen at the site of the *n*th local generator now consists of the subsystem *C* and the dynamic equivalent of Figure 2(b). Therefore, the localized power system (LPS) model takes the form shown in Figure 3. Here, δ_n, M_n, and P_{mn} are respectively the rotor angle, inertia constant, and mechanical input power of the local generator. The swing equation of the local generator is given by

$$\dot{\delta}_n = \omega_n \quad (10a)$$

$$M_n\dot{\omega}_n = P_{mn} - P_{en} = P_m - E_n^2 G'_{n,n} - E_n E_T[G'_{n,T}\cos(\delta_n - \delta_T) + B'_{n,T}\sin(\delta_n - \delta_T)] \quad (10b)$$

and that of the equivalent generator is given by

$$\dot{\delta}_T = \omega_T \quad (11a)$$

$$M_T\dot{\omega}_T = P_T - P_{eT} = P_T - E_T^2 G'_{T,T} - E_T E_n[G'_{T,n}\cos(\delta_T - \delta_n) + B'_{T,n}\sin(\delta_T - \delta_n)] \quad (11b)$$

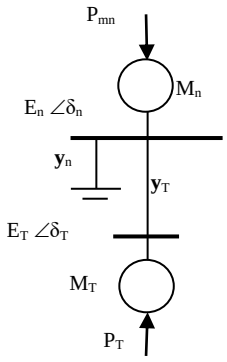

Figure 3. Localized power system (LPS) model at the site of *n*th generator

Here, P_{en} and P_{eT} are respectively the output electrical powers of the local generator and the equivalent generator. Further, ($G'_{n,n}+ j\, B'_{n,n}$), ($G'_{T,T}+j\, B'_{T,T}$), ($G'_{n,T}+j\, B'_{n,T}$) and ($G'_{T,n}+j\, B'_{T,n}$) are elements of the admittance matrix of the localized power system shown in Figure 3, and ω_n and ω_T are respectively the speeds of the local generator and the equivalent generator. The dynamics of the system described by (10) and (11) can be put in the two-state form of representation as:

$$\omega = \dot{\delta} \tag{12a}$$

$$\dot{\omega} = M_n^{-1}(P_{mn} - P_{en}) - M_T^{-1}(P_T - P_{eT}) \tag{12b}$$

where

$$P_{en} = E_n^2 G'_{n,n} + E_n E_T [G'_{n,T} \cos\delta + B'_{n,T} \sin\delta] \tag{12c}$$

$$P_{eT} = E_T^2 G'_{T,T} + E_T E_n [G'_{T,n} \cos\delta - B'_{T,n} \sin\delta] \tag{12d}$$

$$\delta = \delta_n - \delta_T \tag{12e}$$

with δ and ω as the state variables. The localized two-generator system described by (12) is referred to as the *n*th localized power system. Since δ and ω respectively represent the separation angle and speed of an individual generator with respect to its respective remaining generators, the trajectories of a localized power system (LPS) can also be referred to as the separation trajectories of the corresponding individual generator.

Note that the two-generator localized model at the site of a local generator describes the dynamic behavior of the full power system as it is seen at the site of the local generator. Therefore, these localized power system models are not subsystems like the interconnected subsystems in a power system where the entire power system can be unstable even though each subsystem is stable.

2.3. Transient stability of full system and the localized power systems

Consider that the full power system after a major disturbance, reaches its appropriate stable equilibrium point in the post-fault configuration. Then all the generators are coherent i.e. they operate at the same speed which is not necessarily the synchronous speed. This can be written as

$$\dot{\delta}_1 = \dot{\delta}_2 = \cdots = \dot{\delta}_n \tag{13}$$

Now consider the behavior of the LPS corresponding to the *n*th local generator, as the full system reaches the equilibrium state. By (13), the remaining generators are coherent i.e.

$$\dot{\delta}_1 = \dot{\delta}_2 = \cdots = \dot{\delta}_{n-1} = \dot{\lambda} \text{ (say)} \tag{14a}$$

where $\dot{\lambda}$ is the speed of the remaining generators. Since the angular difference between any two remaining generators is constant, it can be shown using (6) that E_T is a constant quantity i.e.

$$\dot{E}_T = 0 \tag{14b}$$

Equation (6) can also be written as

$$E_T e^{j\delta_T} = \left(\sum_{k\in D_l} \mathbf{Y}_{nk} E_k e^{j\delta_k}\right) / \left(\sum_{k\in D_l} \mathbf{Y}_{nk}\right) \tag{15}$$

Differentiation of (15) leads to

$$E_T e^{j\delta_T} \dot{\delta}_T = \left(\sum_{k\in D_l} \mathbf{Y}_{nk} E_k e^{j\delta_k} \dot{\delta}_k\right) / \left(\sum_{k\in D_l} \mathbf{Y}_{nk}\right) \tag{16}$$

Use of (14a) in (16) leads to

$$E_T e^{j\delta_T}\dot{\delta}_T = \dot{\lambda}(\sum_{k\in D_l}\mathbf{Y}_{nk}E_k e^{j\delta_k})/(\sum_{k\in D_l}\mathbf{Y}_{nk}) \quad (17)$$

From (15) and (17), it can be easily shown that

$$\dot{\delta}_T = \dot{\lambda} \quad (18)$$

which indicates that the speed of the equivalent generator is same as the speed of the remaining generators.

However, at stable equilibrium point of the full system, the speed of the *n*th generator is also equal to the speed of the remaining generators as indicated in (13). This leads to the following.

$$\dot{\delta}_n = \dot{\lambda} = \dot{\delta}_T \quad (19a)$$

i.e.

$$\omega = \dot{\delta}_n - \dot{\delta}_T = \dot{\delta} = 0 \quad (19b)$$

Since the LPS speed ω is zero, the LPS acceleration is also zero i.e.

$$\dot{\omega} = 0 \quad (19c)$$

Differentiation of (12c) and (12d) leads to

$$\dot{P}_{en} = 0\,,\ \dot{P}_{eT} = 0 \quad (19d)$$

Use of (19c) in (12b) and then its differentiation leads to

$$\dot{P}_T = 0 \quad (19e)$$

However, equation (19b) combined with (19c) i.e. ($\omega = 0$, $\dot{\omega} = 0$) defines the stable equilibrium of the LPS. Therefore, when the full system reaches its stable equilibrium, then the *n*th LPS also reaches its stable equilibrium. But this is true for each of the localized power systems. Therefore, all the localized power systems reach their respective stable equilibriums as the full system reaches its appropriate stable equilibrium in the sense that all the generators run at the same speed that is not necessarily the synchronous speed. In other words, it can be said that if each of the localized power systems is at its respective stable equilibrium, then the full system is at its appropriate stable equilibrium. This is the basis of the proposed transient stability method. This basis is also supported by the investigative test results. Therefore, in terms of localized control of transient stability by the proposed method, if each of the localized power systems is driven independently by local control actions to its respective stable equilibrium, then the full power system is driven to its stable equilibrium.

As indicated here, if each LPS is stable, then the full system is stable. However, the stability of an LPS also means the stability of its local generator with respect to the remaining generators. Therefore, according to the proposed method, if each of the individual generators is stable in terms of its corresponding LPS trajectories, then the full system is stable. Since each of the LPS trajectories is involved in the transient stability studies, the proposed method captures all the transient stability phenomena of the full system. This is also supported by the test results based on the comparison of transient stability assessment results by the proposed method with those by the SBS method. Therefore, in the proposed LTS method, the LPS trajectories can be used to assess transient stability of the full system in terms of critical clearing time (CCT). This has been discussed in [31]. However, as indicated earlier, the proposed method is not intended for transient stability assessment. It is intended solely for real-time localized control of transient stability.

3. REAL-TIME LOCALIZED CONTROL OF TRANSIENT STABILITY BY LTS METHOD

The use of the proposed method for real-time localized control of transient stability is described here. In terms of local control, if each LPS is driven to its respective stable equilibrium i.e. if each LPS trajectory is stabilized by local control actions, then the full system is driven to its stable equilibrium. With the known post-fault passive network model of the external system (the system external to the network at the local generator site) and the total inertia constant of the remaining generators, all the unknown variables of an

LPS can be estimated from local information and real-time measurement data taken solely at the corresponding local generator site as discussed later. Therefore, it is assumed that the latest updated pre-fault passive network model of the external system, fault information including the fault clearing time, and total inertia constant of the remaining generators are known at the site of any individual generator. All these can be obtained directly from the main computer of the system control center. With the knowledge of the pre-fault passive network model of the external system, fault information, and the local network, the post-fault reduced admittance matrix can be obtained easily. Then the admittance parameters $\mathbf{y}_n$ and $\mathbf{y}_T$ of the LPS model can be determined.

However, to apply this method, as described in [31], it is essential that the local control actions (if any) at different generator sites are applied during the same time step such that there is no local control action present in the full system at the beginning of any particular time step. This is necessary to ensure that the post-fault system returns to the original post-fault system at the beginning of any particular time step. Therefore, it is assumed that each generator site uses the fault clearing time as a common reference time so that the beginning and ending of the time steps used by each generator site are same. As such, the post-fault system returns to the original post-fault system at the beginning of each time step. At the beginning of a particular time step, necessary local computations are done independently at each local generator site using the respective original post-fault passive network model. However, the necessary local control actions (if any) at different generator sites are applied during the same time step. Note that the different local control means including the FACTS devices can be easily integrated into the network model of the local generator site for the purpose of control. With the admittance parameters $\mathbf{y}_n$ and $\mathbf{y}_T$ of an LPS model known, the different unknown variables of the LPS can be estimated from real-time local measurement data as follows.

Consider the *n*th LPS. With known resistance and direct axis transient reactance of *n*th local generator, voltage E_n, real power P_{en}, and the reactive power Q_{en} at the internal bus can be determined using measurement data like the real power, reactive power, and voltage magnitude taken at its external bus. However, P_{en} and Q_{en} in terms of the LPS quantities are given by

$$P_{en} = E_n^2 G'_{n,n} + E_n E_T [G'_{n,T} \cos\delta + B'_{n,T} \sin\delta] \tag{20a}$$

$$Q_{en} = -E_n^2 B'_{n,n} + E_n E_T [G'_{n,T} \sin\delta - B'_{n,T} \cos\delta] \tag{20b}$$

which can be solved to yield

$$\delta = \tan^{-1}(Q'/P') + \beta \tag{21a}$$

where

$$P' = P_{en} - E_n^2 G'_{n,n}, \qquad Q' = Q_{en} + E_n^2 B'_{n,n} \tag{21b}$$

$$\beta = \tan^{-1}(B'_{n,T}/G'_{n,T}) \tag{21c}$$

So, the LPS angle δ can be determined by (21) with P_{en} and Q_{en} obtained from measurement data. However, the angle δ obtained from (21) must be adjusted by the addition or subtraction of an integer number times 2π electrical radians for pole slippage to obtain the LPS angular trajectory corresponding to the local generator. Therefore, the LPS angle δ can be determined by (21) with proper adjustment of δ as indicated. With known values of δ at some suitable time steps, δ can be approximated by a third degree polynomial and then both ω and $\dot{\omega}$ can be estimated from its derivatives. More details are provided later. Equations (20a) and (20b) can also be solved to yield

$$E_T = (1/E_n)\sqrt{(P'^2 + Q'^2)/(G'^2_{n,T} + B'^2_{n,T})} \tag{22}$$

Therefore, E_T can be determined using (21b) and (22). P_{eT} can now be obtained from (12d). P_{mn} can be obtained from the pre-fault steady-state real power P_{en} since they are equal. P_T can now be determined from (12b) by matching the estimated value of LPS acceleration $\dot{\omega}$. Therefore, P_T is given by

$$P_T = (M_T/M_n)(P_{mn} - P_{en}) - \dot{\omega} M_T + P_{eT} \tag{23}$$

with known local generator inertia constant M_n and total inertia constant M_T of the remaining generators.

It can be seen here that with the known post-fault passive network model of the external system and the total inertia constant of the remaining generators, all the unknown variables (E_T, δ and P_T) of the LPS model shown in Figure 3 can be computed from measured data taken solely at the external terminal of the local generator. Therefore, this LPS model can be used to design and implement real-time localized control strategies that can drive the LPS to its stable equilibrium point.

At any instant of time, a stable equilibrium point of the LPS described by (12) can be defined by holding E_T and P_T fixed at their current estimated values. This stable equilibrium state (δ_e, 0) is referred to as the instantaneous stable equilibrium state. Here, δ_e is the instantaneous stable LPS angle that can be obtained from (12b) by setting its left side equal to zero and using (12c) and (12d). However, if the values of E_T and P_T sustain, the instantaneous stable equilibrium becomes the stable equilibrium of the LPS. Note that since E_T and P_T are held fixed, δ_e is also fixed i.e. $\dot{\delta}_e$ is zero. In terms of local control, if each of the localized power systems is driven from its current state (δ, ω) to the instantaneous stable equilibrium point (δ_e, 0) of its respective state-space, then the full system is driven to its stable equilibrium. Therefore, the real-time local control of transient stability by the proposed method can be easily implemented at the site of each local generator independently without requiring any coordination.

4. RESULTS ON REAL-TIME LOCALIZED CONTROL OF TRANSIENT STABILITY USING BRAKING RESISTORS AS THE LOCAL CONTROL MEANS

The potential of the LTS method for use in real-time localized control of transient stability was investigated on the well-known New England 39-bus 10-generator system. In this investigation, braking resistors were used as the local control means. A number of three-phase short circuit faults were considered. These results on real-time localized control of transient stability are presented here. In this investigation, local computations with SBS simulated local measurement data were used to compute the necessary local controls. These local controls were then applied to improve the CCT ranges. In all the SBS simulations, a time-step size of 0.01 s has been used. However, to determine the local controls required to drive the localized power systems to their respective equilibriums i.e. to stabilize the LPS trajectories, optimal aim control strategy [32] was chosen due to its suitability for two-generator systems. With reference to local control of power systems, this optimal aim strategy (OAS) is described in detail in [25] where this strategy is referred to as a Localized Aiming Strategy (LAS). With respect to a two-generator system, this strategy has also been described in [33].

For the purpose of localized control by the LTS method using OAS, the control dependent dynamic equations of the *n*th localized power system are written in the form as

$$\omega = \dot{\delta}, \qquad \dot{\omega} = [P_m - P_e + U_n(t)]/M \tag{24}$$

where $M = M_n M_T/(M_n + M_T)$, $P_m = (P_{mn} M_T - M_n P_T)/(M_n + M_T)$ and $P_e = (P_{en} M_T - M_n P_{eT})/(M_n + M_T) = f(\delta)$. Here, $U_n(t)$ represents an additive power control in the localized power system. However, the additive power u_n that is required by the *n*th local generator to produce the additive power U_n in the localized power system is given by

$$u_n(t) = MU_n(t)/M_n \tag{25}$$

This power is in addition to P_{mn}. However, since this additive power is a negative quantity, it also means that $\Delta P_{en} = -u_n(t)$ is an equivalent additional electrical output power of the local generator. Therefore, the new electrical output power required by the local generator to stabilize its respective LPS is given by

$$P_{en}^{new} = P_{en} + \Delta P_{en} \tag{26}$$

Other details can be found in [25], [33].

In this investigation, the value of $\dot{\omega}$ required to estimate P_T and the value of ω required in OAS at the beginning of a time-step have been determined from the derivatives of a third degree polynomial approximation obtained by matching the LPS angle at current time and the LPS angles at three previous times. Note that this estimation process has not been used for estimation at future times. Assuming that the measurement data and hence the LPS angle δ was available at the beginning of the post-fault configuration,

there was a delay of three time-steps to initiate the control. At the beginning of a current time step after three previous time-steps in the post-fault configuration, the additional electrical output powers required by the different local generators were computed by OAS and they were then applied over the entire length of the current time-step. However, the additional electrical output power required by a local generator was obtained by applying braking resistors at an arbitrarily chosen bus of the local generator site. For the local sites of generators 1-9, braking resistors were applied at the high tension sides of the step-up transformers as shown in Figure 4. However, for the local site of generator 10, braking resistors were applied at the generator external bus.

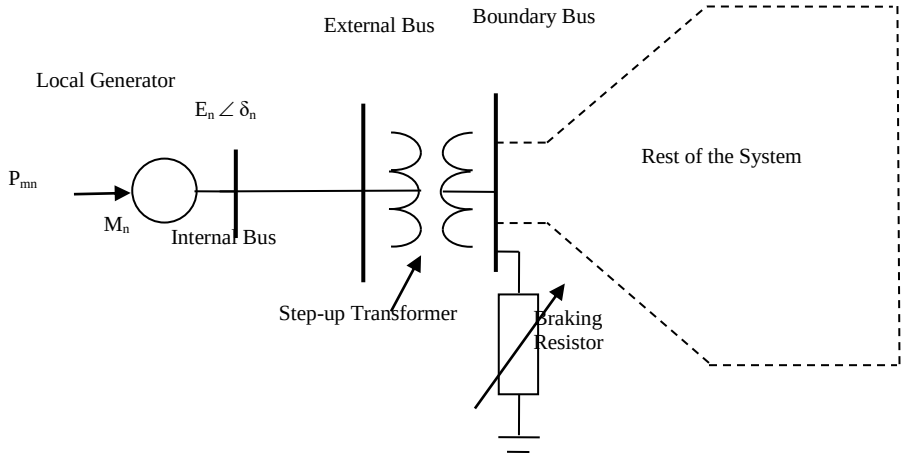

Figure 4. Power system at the site of *n*th local generator with shunt braking resistor

The test results for seven different fault cases are presented here. The critical clearing time (CCT) ranges for these fault cases were determined by SBS method using the COA frame of reference. In each fault case, the CCT ranges were obtained without local controls applied as well as with local controls applied. However, as indicated earlier, braking resistors were used in each of the fault cases as the local control means. Further, the SBS trajectories corresponding to the critically stable conditions with local controls applied are presented for the first six fault cases.

Fault Case I: A three-phase short circuit fault on bus 29 was cleared by removing line 29-26. Without any local control applied, the system was found to be stable at a fault clearing time of 0.07 s and unstable at a fault clearing time of 0.08 s. So the CCT range without local controls applied was (0.07 s-0.08 s). However, with local controls applied, the system was found to be stable at a fault clearing time of 0.15 s and unstable at a fault clearing time of 0.16 s. Therefore, the CCT range with local controls applied improved to (0.15 s-0.16 s). This is a very significant improvement. The SBS trajectories corresponding to the critically stable condition for this fault (i.e. at the fault clearing time of 0.15 s) with local controls applied are shown in Figure 5.

Fault Case II: A three-phase short circuit fault on bus 25 was cleared by removing line 25-2. Without any local control applied, the system was found to be stable at a fault clearing time of 0.13 s and unstable at a fault clearing time of 0.14 s. So the CCT range without local controls applied was (0.13 s-0.14 s). However, with local controls applied, the system was found to be stable at a fault clearing time of 0.20 s and unstable at a fault clearing time of 0.21 s. Therefore, the CCT range with local controls applied improved to (0.20 s-0.21 s). This is also a very significant improvement. The SBS trajectories corresponding to the critically stable condition for this fault (i.e. at the fault clearing time of 0.20 s) with local controls applied are shown in Figure 6.

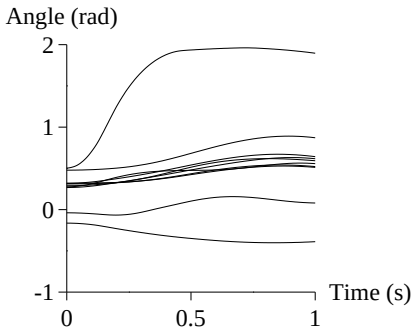

Figure 5. Controlled SBS trajectories for fault case I with fault clearing time of 0.15 s

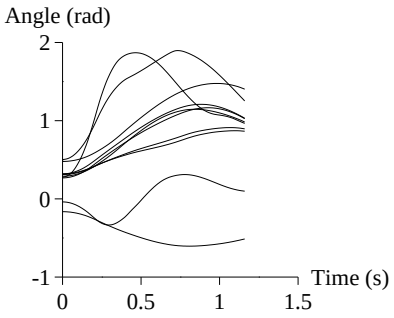

Figure 6. Controlled SBS trajectories for fault case II with fault clearing time of 0.20 s

Fault Case III: A three-phase short circuit fault on bus 22 was cleared by removing line 22-21. Without any local control applied, the CCT range was found to be (0.17 s-0.18 s). However, with local controls applied, the CCT range improved to (0.25 s-0.26 s). The SBS trajectories corresponding to the critically stable condition for this fault (i.e. at the fault clearing time of 0.25 s) with local controls applied are shown in Figure 7.

Fault Case IV: A three-phase short circuit fault on bus 24 was cleared by removing line 24-23. Without any local control applied, the CCT range was found to be (0.20 s-0.21 s). However, with local controls applied, the CCT range improved to (0.24 s-0.25 s). The SBS trajectories corresponding to the critically stable condition for this fault (i.e. at the fault clearing time of 0.24 s) with local controls applied are shown in Figure 8.

Fault Case V: A three-phase short circuit fault on bus 27 was cleared by removing line 27-17. Without any local control applied, the CCT range was found to be (0.18 s-0.19 s). However, with local controls applied, the CCT range improved to (0.26 s-0.27 s). The SBS trajectories corresponding to the critically stable condition for this fault (i.e. at the fault clearing time of 0.26 s) with local controls applied are shown in Figure 9.

Fault Case VI: A three-phase short circuit fault on bus 10 was cleared by removing line 10-13. Without any local control applied, the CCT range was found to be (0.22 s-0.23 s). However, with local controls applied, the CCT range improved to (0.25 s-0.26 s). The SBS trajectories corresponding to the critically stable condition for this fault (i.e. at the fault clearing time of 0.25 s) with local controls applied are shown in Figure 10.

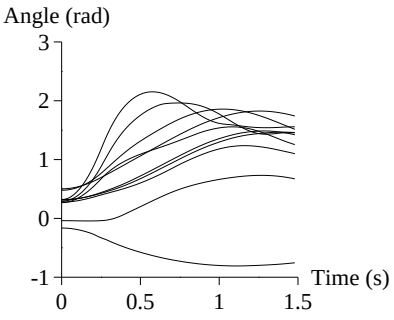

Figure 7. Controlled SBS trajectories for fault case III with fault clearing time of 0.25 s

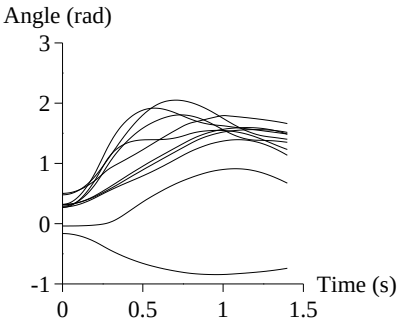

Figure 8. Controlled SBS trajectories for fault case IV with fault clearing time of 0.24 s

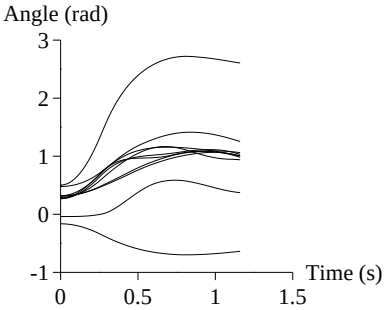

Figure 9. Controlled SBS trajectories for fault case V with fault clearing time of 0.26 s

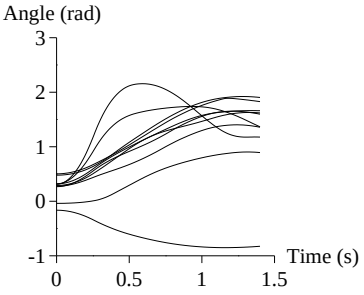

Figure 10. Controlled SBS trajectories for fault case VI with fault clearing time of 0.25 s

Fault Case VII: A three-phase short circuit fault on bus 15 was cleared by removing line 15-14. Without any local control applied, the CCT range was found to be (0.23 s-0.24 s). However, with local controls applied, the CCT range improved to (0.27 s-0.28 s).

The summary of the test results without local controls applied and with local controls applied are shown in Table 1 for comparison. As it can be seen from this table, the results are very promising and they show very good improvement of transient stability in terms of CCT ranges by the real-time localized control. These results clearly demonstrate the high potential of the proposed method for use in real-time localized control of transient stability.

Table 1. CCT Ranges without and with Localized Controls Applied

Fault Cases	Line tripped between buses *Faulty bus	CCT ranges (s)	
		Without control	With control
Case I	*29 – 26	0.07-0.08	0.15-0.16
Case II	*25-2	0.13-0.14	0.20-0.21
Case III	*22-21	0.17-0.18	0.25-0.26
Case IV	*24-23	0.20-0.21	0.24-0.25
Case V	*27-17	0.18-0.19	0.26-0.27
Case VI	*10-13	0.22-0.23	0.25-0.26
Case VII	*15-14	0.23-0.24	0.27-0.28

5. CONCLUSION

A new methodology based on a completely new idea of localized transient stability, is presented solely for use in real-time localized control of transient stability. In this localized transient stability (LTS) method, transient stability is viewed as the interaction of each individual generator with its respective remaining generators. Therefore, the method uses a two-generator localized power system (LPS) model at the site of each individual generator. In this method, if each LPS is stable, then the full power system is stable. Therefore, in terms of localized control of transient stability, if each LPS is driven to its respective stable equilibrium using local measurements and computations with local control actions, then the entire power system is driven to its appropriate stable equilibrium. As discussed in this paper, the proposed method overcomes the serious drawbacks of the different localized control strategies proposed in the literature. Therefore, the system equilibrium state in the proposed method refers to a state at which all the generators run at the same speed that is not necessarily the synchronous speed. The method also provides dynamic equations for the remaining generators, which are necessary to design effective localized control strategies that can drive the power system to its appropriate equilibrium. The test results presented here with the braking resistors as local control means show very good improvement of transient stability in terms of CCT ranges. These results clearly demonstrate the high potential of the proposed method for use in real-time localized control of transient stability. The use of the proposed method in the real-time localized control of transient stability with FACTS devices as the local control means is under investigation. However, the real-time localized control by the proposed method requires further investigation using the other control strategies (i.e. control strategies other than the optimal aim strategy) with different local control means.

ACKNOWLEDGEMENTS

Some of the materials presented here are based upon work that is supported by the National Institute of Food and Agriculture, U.S. Department of Agriculture, Evans-Allen project number SCX-313-02-15.

REFERENCES

[1] A. A. Fouad and V. Vittal, "Power System Transient Stability Using the Transient Energy Function Method," (Prentice-Hall, 1992).
[2] Y. Xue, T. Van Custem and M. Ribbens-Pavella, "Extended equal area criterion justifications, generalizations, applications," in *IEEE Transactions on Power Systems*, vol. 4, no. 1, pp. 44-52, Feb. 1989.
[3] V. Vittal, P. Sauer, S. Meliopoulos, and G. K. Stefopoulos, "On-line transient stability assessment scoping study," Final Project Report, PSERC Publication 05-04, Power Systems Engineering Research Center (PSERC), 2005.
[4] A. M. Miah, "Study of a coherency-based simple dynamic equivalent for transient stability assessment," in *IET Generation, Transmission & Distribution*, vol. 5, no. 4, pp. 405-416, April 2011.
[5] A. M. Miah, "Comparative study on the performance of a coherency-based dynamic equivalent with the new inertial aggregation," *International Journal of Applied Power Engineering*, vol. 1, no. 3, pp. 105-114, December 2012.
[6] A. M. Khalil and R. Iravani, "A Dynamic Coherency Identification Method Based on Frequency Deviation Signals," in *IEEE Transactions on Power Systems*, vol. 31, no. 3, pp. 1779-1787, May 2016.
[7] N. Yorino, E. Popov, Y. Zoka, Y. Sasaki and H. Sugihara, "An Application of Critical Trajectory Method to BCU Problem for Transient Stability Studies," in *IEEE Transactions on Power Systems*, vol. 28, no. 4, pp. 4237-4244, Nov. 2013.
[8] J. N. Rai, N. Hasan, B. B. Arora, "Comparison of FACTS devices for two area power system stability enhancement using MATLAB modelling." *International Journal of Applied Power Engineering*, vol. 3, no. 2, pp. 130-139, August 2014.
[9] S. Zhao, H. Jia, D. Fang, Y. Jiang and X. Kong, "Criterion to evaluate power system online transient stability based on adjoint system energy function," in *IET Generation, Transmission & Distribution*, vol. 9, no. 1, pp. 104-112, 8 1 2015.
[10] T. L. Vu and K. Turitsyn, "Lyapunov Functions Family Approach to Transient Stability Assessment," in *IEEE Transactions on Power Systems*, vol. 31, no. 2, pp. 1269-1277, March 2016.
[11] F. Milano, "Semi-Implicit Formulation of Differential-Algebraic Equations for Transient Stability Analysis," in *IEEE Transactions on Power Systems*, vol. 31, no. 6, pp. 4534-4543, Nov. 2016.
[12] M. Oluic, M. Ghandhari and B. Berggren, "Methodology for Rotor Angle Transient Stability Assessment in Parameter Space," in *IEEE Transactions on Power Systems*, vol. 32, no. 2, pp. 1202-1211, March 2017.
[13] H. Bosetti and S. Khan, "Transient Stability in Oscillating Multi-Machine Systems Using Lyapunov Vectors," in *IEEE Transactions on Power Systems*, vol. 33, no. 2, pp. 2078-2086, March 2018.
[14] V. Jalili-Marandi, Z. Zhou and V. Dinavahi, "Large-Scale Transient Stability Simulation of Electrical Power Systems on Parallel GPUs," in *IEEE Transactions on Parallel and Distributed Systems*, vol. 23, no. 7, pp. 1255-1266, July 2012.
[15] Y. Liu and Q. Jiang, "Two-Stage Parallel Waveform Relaxation Method for Large-Scale Power System Transient Stability Simulation," in *IEEE Transactions on Power Systems*, vol. 31, no. 1, pp. 153-162, Jan. 2016.
[16] M. A. Tomim, J. R. Martí and J. A. Passos Filho, "Parallel Transient Stability Simulation Based on Multi-Area Thévenin Equivalents," in *IEEE Transactions on Smart Grid*, vol. 8, no. 3, pp. 1366-1377, May 2017.
[17] J. Yan, C. Liu and U. Vaidya, "PMU-Based Monitoring of Rotor Angle Dynamics," in *IEEE Transactions on Power Systems*, vol. 26, no. 4, pp. 2125-2133, Nov. 2011.
[18] J. C. Cepeda, J. L. Rueda, D. G. Colomé and D. E. Echeverría, "Real-time transient stability assessment based on centre-of-inertia estimation from phasor measurement unit records," in *IET Generation, Transmission & Distribution*, vol. 8, no. 8, pp. 1363-1376, 2014.
[19] S. Dasgupta, M. Paramasivam, U. Vaidya and V. Ajjarapu, "PMU-Based Model-Free Approach for Real-Time Rotor Angle Monitoring," in *IEEE Transactions on Power Systems*, vol. 30, no. 5, pp. 2818-2819, Sept. 2015.
[20] Y. Wu, M. Musavi and P. Lerley, "Synchrophasor-Based Monitoring of Critical Generator Buses for Transient Stability," in *IEEE Transactions on Power Systems*, vol. 31, no. 1, pp. 287-295, Jan. 2016.
[21] P. Bhui and N. Senroy, "Real-Time Prediction and Control of Transient Stability Using Transient Energy Function," in *IEEE Transactions on Power Systems*, vol. 32, no. 2, pp. 923-934, March 2017.
[22] M. Glavic, D. Ernst, D. Ruiz-Vega, L. Wehenkel and M. Pavella, "E-SIME-A method for transient stability closed-loop emergency control: achievements and prospects," *2007 iREP Symposium-Bulk Power System Dynamics and Control-VII. Revitalizing Operational Reliability*, Charleston, SC, 2007, pp. 1-10.
[23] G. C. Zweigle and V. Venkatasubramanian, "Wide-Area Optimal Control of Electric Power Systems With Application to Transient Stability for Higher Order Contingencies," in *IEEE Transactions on Power Systems*, vol. 28, no. 3, pp. 2313-2320, Aug. 2013.
[24] J. Zaborszky, A. Subramanian, Tzyh-Jong Tarn and Keh-Ming Lu, "A new state space for emergency control in the interconnected power system," in *IEEE Transactions on Automatic Control*, vol. 22, no. 4, pp. 505-517, August 1977.
[25] J. Meisel, and R. D. Barnard, "*Transient-stability augmentation using a localized aiming-strategy algorithm*," in Proc. Power System Computation Conference V, Cambridge, England, paper no. 3.2/9, 1975.

[26] J. Meisel, A. Sen, and M. L. Gilles, "Alleviation of a transient stability crisis using shunt braking resistors and series capacitors," *Electrical Power & Energy Systems*, vol. 3, no. 1, pp. 25-37, January 1981.
[27] R. Patel, T. S. Bhatti and D. P. Kothari, "Improvement of power system transient stability by coordinated operation of fast valving and braking resistor," in *IEE Proceedings-Generation, Transmission and Distribution*, vol. 150, no. 3, pp. 311-316, 13 May 2003.
[28] M. H. Haque, "Improvement of first swing stability limit by utilizing full benefit of shunt FACTS devices," in *IEEE Transactions on Power Systems*, vol. 19, no. 4, pp. 1894-1902, Nov. 2004.
[29] M. H. Haque, "Damping improvement by FACTS devices: A comparison between STATCOM and SSSC," *J. of Electric Power Systems Research*, vol. 76, pp. 865-872, June 2006.
[30] M. H. Haque, "Application of UPFC to Enhance Transient Stability Limit," *2007 IEEE Power Engineering Society General Meeting*, Tampa, FL, 2007, pp. 1-6.
[31] A. M. Miah, "A new methodology for the purpose of real-time local control of transient stability," *2014 IEEE PES T&D Conference and Exposition*, Chicago, IL, 2014, pp. 1-5.
[32] R. Barnard, "An optimal-aim control strategy for nonlinear regulation systems," in *IEEE Transactions on Automatic Control*, vol. 20, no. 2, pp. 200-208, April 1975.
[33] A. M. Miah, "Local control of transient stability by optimal aim strategy," in *Proc. Third International Conference on Electrical & Computer Engineering*, Dhaka, Bangladesh, December 28-30, 2004, pp. 171-174.

BIOGRAPHY OF AUTHORS

Abdul Malek Miah received the B.Sc. and M.Sc. degrees in Electrical Engineering from the Bangladesh University of Engineering and Technology in 1969 and 1981 respectively, and the Ph.D. degree in electrical engineering from the Wayne State University, Michigan, USA, in 1992. He worked in industries for several years. He was also with the faculty of Bangladesh University of Engineering and Technology. He joined the South Carolina State University in 1990 and is currently a Professor of Electrical Engineering Technology. His current research interest is in the area of localized transient stability and control.